Technical Document 2453
March 1993

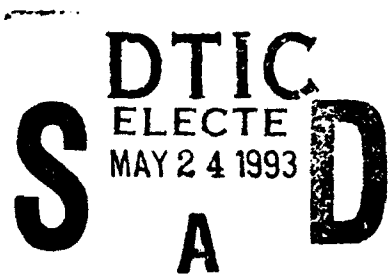

Application of Integral and Differential Equation Methods for Various EM Interaction Problems

University of South Carolina

Technical Document 2453
March 1993

Application of Integral and Differential Equation Methods for Various EM Interaction Problems

University of South Carolina

NAVAL COMMAND, CONTROL AND OCEAN SURVEILLANCE CENTER
RDT&E DIVISION
San Diego, California 92152-5001

J. D. FONTANA, CAPT, USN
Commanding Officer

R. T. SHEARER
Executive Director

ADMINISTRATIVE INFORMATION

Faculty members from the University of South Carolina conducted this study for the Electromagnetic Technology and Systems Branch (Code 824) at the Naval Command, Control and Ocean Surveillance Center, RDT&E Division, San Diego, California 92152-5001, as part of the 1992 ASEE-US Navy summer faculty research program. Benjamin Beker of the Department of Electrical and Computer Engineering at the University of South Carolina wrote this technical document.

This document partially fulfills Milestone 2, Task Number 4 (EM Technologies for the Composite Mast), of the Electromagnetic Compatibility Project (RH21C13) of the Surface Ship Technology Block Program. The Office of Naval Technology, Arlington, Virginia 22217-5000, sponsored this study. The technology area manager at the Office of Naval Technology was J. E. Gagorik (ONT-211).

Released by
J. B. Rhode, Head
Electromagnetic Technology
and Systems Branch

Under authority of
R. J. Kochanski, Head
Communications Systems
Engineering and Integration
Division

DM

Abstract

This report reviews the application of integral equation methods that are commonly employed to study interaction of EM fields with two-dimensional lossy anisotropic objects. The study partially focuses on plane wave scattering by arbitrarily shaped cylindrical geometries with circular and rectangular cross-sections. In addition to solid material objects, investigation of the bistatic radar cross section of several metallic circular cylinders, coated with a single layer of anisotropic material, is also presented. Finally, radiation effects from a uniform line source through a lossy anisotropic shell of finite thickness are also investigated.

The report includes an overview of the theoretical formulation of the problem in terms of the combined-field surface integral equations (CFSIEs). The highligths of the Method of Moments numerical solution to CFSIEs are given, and numerical results for solid, hollow, and coated cylindrical scatterers are presented. The emphasis in the discussion of the numerical results is placed on the effects of material anisotropy in the EM response of the scatterer.

Acknowledgment

The author wishes to thank James C. Logan, Code 824, of NRaD for many helpful discussions regarding the numerical results appearing in this report. Thanks are also extended to Thinh Q. Ho of NRaD for providing measured values of complex dielectric constants of several composite materials used in this study. The author is also grateful to Daniel Tam, Code 824, of NRaD for access to computer resources that were used to generate all data appearing in this report.

Table of Contents

Section 1

INTRODUCTION

Numerical modeling of EM interaction is normally performed by using either differential or integral equation methods. Both techniques can be implemented to solve problems in frequency or time domain. The method of moments (MOM) approach (Harrington, 1968) to solving integral equations has matured to the point where it can be used to solve very complex problems. In the past, MOM has only been applied to scattering and radiation problems involving perfectly conducting or isotropic penetrable, lossy or losses objects. However, many materials such as, for example, composites that are used today in practical applications exhibit anisotropy properties.

The attractive features of composite media include the combination of their mechanical agility and correspondingly desirable electromagnetic properties. They are much lighter than the metal and exhibit comparable strength. Since Navy surface ships are built primarily from the metal, they are beginning to reach their weight limitations. In order to consider composite materials as alternatives to the metal for replacing portions of the ship's superstructure, detailed studies of their electromagnetic properties are needed. Since such materials are anisotropic, effective numerical tools to study their interaction with electromagnetic fields are required.

To account for these effects, several integral equation formulations for scattering and radiation by anisotropic objects have been developed recently (Graglia et al., 1987; Monzon, 1988; Beker et al., 1989). Integral equations are usually separated into those that are of volumetric or surface kind. Although the volumetric integral equations (Graglia et al., 1987) are very general and can be used to analyze scatterers composed of conductors imbedded in anisotropic or inhomogenous media, they require solution to matrix equations with a very large number of unknowns. The surface integral equations, on the other hand, are best suited to effectively predict the scattering response from homogeneous objects. However, partially inhomogeneous objects can be analyzed employing CFSIEs as well. In this case, the entire region of interest must be subdivided into multiple locally homogeneous subregions with appropriate boundary conditions

enforced to connect them together. Despite the added complexity, a great deal of information about the interaction of inhomogeneous anisotropic materials with externally generated EM fields can still be obtained by employing them.

This report is aimed at examining the effects that material anisotropy has on scattering properties of arbitrarily shaped solid, hollow, and coated two-dimensional objects. Numerical results are provided for the far-fields of lossless as well as lossy scatterers. In addition, the radiation patterns due to a line source placed inside a lossy anisotropic circular shell which are functions of material anisotropy are also included. The surface integral equations for all aforementioned geometries are solved by using the standard frequency-domain two-dimensional method of moments codes developed at the University of South Carolina (Beker et al., 1989; Beker, March 1991; and Beker et al., 1990).

Although most practical problems are three-dimensional, a great deal of information on the electromagnetic nature of composite media can still be learned from studying two-dimensional geometries. Radiation of a line source placed inside a shell composed of lossy anisotropic material can give an estimate of power loss due to reflections and dissipation in the material. At the same time, scattering from canonical objects such plates or circles gives an idea of how the anisotropy of the material affects the RCS. Consequently, these studies can provide sufficient information to determine preliminary design specifications for the composite materials that can be potentially used for parts of Navy surface ships.

Section 2

INTEGRAL EQUATIONS FOR ANISOTROPIC MEDIA

In this Section the highlights of two kinds of surface integral equations for two-dimensional, homogeneous anisotropic regions are presented. The formulation to several scattering and radiation problems is given and its method of moments solution is briefly discussed. Numerical results that examine effects of material anisotropy on scattering and radiation from arbitrarily shaped objects are provided in the subsequent Section.

2.1 Formulation of Scattering Problems

Consider a homogeneous, anisotropic, and arbitrarily shaped two-dimensional region shown in Fig. 2-1. The medium is assumed to be characterized by the following forms of the permittivity and permeability tensors:

$$\varepsilon_0[\varepsilon_2] = \varepsilon_0 \begin{bmatrix} \varepsilon_{xx} & \varepsilon_{xy} & 0 \\ \varepsilon_{yx} & \varepsilon_{yy} & 0 \\ 0 & 0 & \varepsilon_{zz} \end{bmatrix} \tag{2-1}$$

$$\mu_0[\mu_2] = \mu_0 \begin{bmatrix} \mu_{xx} & \mu_{xy} & 0 \\ \mu_{yx} & \mu_{yy} & 0 \\ 0 & 0 & \mu_{zz} \end{bmatrix}, \tag{2-2}$$

where ε_0 and μ_0 are the permittivity and permeability of free space.

It is well known that two-dimensional fields can be separated into their transverse electric (*TE*) and magnetic (*TM*) parts or polarizations. This allows for the duality to be applied to find one set of fields, say *TE*, if the solution for the other set (*TM*) is already known (Beker et al., 1989). Therefore, the formulation of the scattering or radiation problem in this part of the report will be restricted to the *TM* polarization, with the

results for the *TE* part obtained via duality. In this report, all fields and sources are assumed to have a time-harmonic dependence $e^{j\omega t}$ which will suppressed throughout.

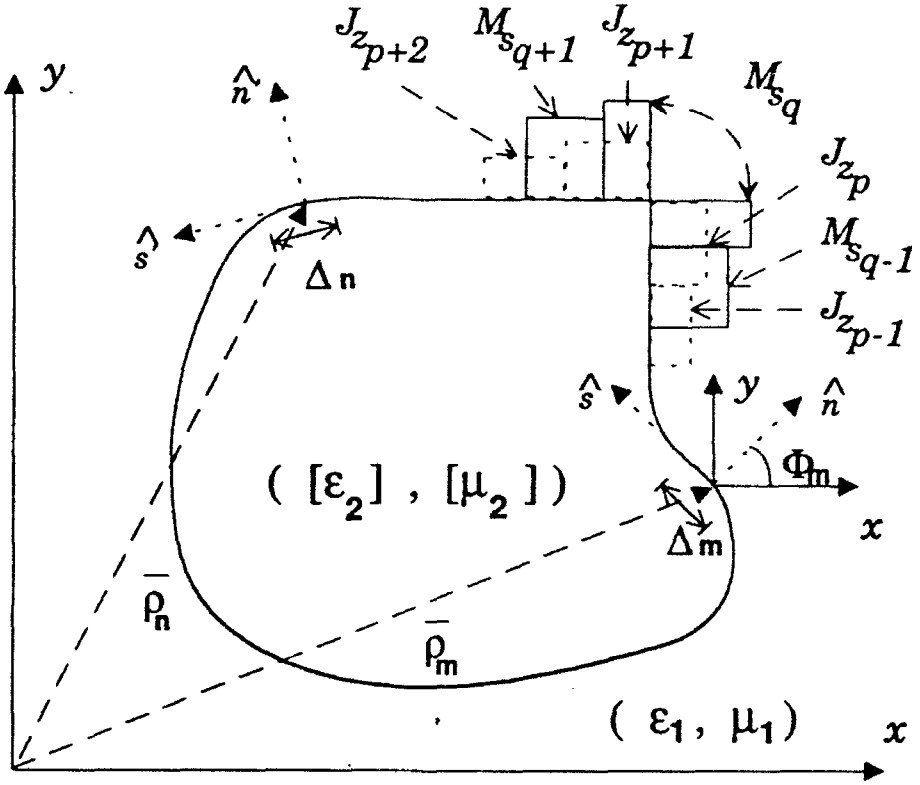

Figure 2-1: Segmented contour of the anisotropic scatterer.

According to (Beker et al., 1990), it is possible to construct the integral equations for anisotropic regions in terms of vector potentials only or to use a mixed (scalar and vector) potential formulation. Consequently, the combined field surface integral equations for a solid (bulk) scatterer shown in Fig. 2-1, exposed to the *TM* excitation, can be written in terms of vector potentials as

$$-E_{z1}^{i} = -j\omega(A_{z1} + A_{z2}) - \hat{z}\cdot\left(\frac{\nabla\times\vec{F}_1}{\varepsilon_0\varepsilon_1} + \frac{[\varepsilon_2]^{-1}\cdot(\nabla\times\vec{F}_2)}{\varepsilon_0}\right) \tag{2-3}$$

$$-\hat{n}\times\vec{H}_1^{i} = -\hat{n}\times\left\{j\omega(\vec{F}_1+\vec{F}_2) + j\omega\nabla\left[\nabla\cdot\left(\frac{\vec{F}_1}{k_1^2} + \frac{[\mu_2]\cdot\vec{F}_2}{k_a^2}\right)\right] - \left(\frac{\nabla\times\vec{A}_1}{\mu_0\mu_1} + \frac{[\mu_2]^{-1}\cdot(\nabla\times\vec{A}_2)}{\mu_0}\right)\right\}, \tag{2-4}$$

where

$$k_1^2 = k_0^2 \varepsilon_1 \mu_1 \tag{2-5}$$

$$k_a^2 = k_0^2 \varepsilon_z \gamma = k_0^2 \varepsilon_z \left(\mu_{xx} \mu_{yy} + \mu_{xy}^2 \right) \quad , \tag{2-6}$$

assuming that $\mu_{yx} = -\mu_{xy}$.

The integral equations for the same problem can also be recast in terms of mixed potentials, which can be achieved with the help of the Lorentz Gauge for anisotropic media (Beker et al., 1990)

$$\psi = \frac{j\omega}{k_a^2} \nabla \cdot \left([\mu_2] \cdot \vec{F}_2 \right) \quad . \tag{2-7}$$

As a result, equation (2-3) still remains the same, but equation (2-4) now becomes

$$-\hat{n} \times \vec{H}_1^i = -\hat{n} \times \left\{ j\omega \left(\vec{F}_1 + \vec{F}_2 \right) + \nabla \left(\psi_1 + \psi_2 \right) - \left(\frac{\nabla \times \vec{A}_1}{\mu_0 \mu_1} + \frac{[\mu_2]^{-1} \cdot \left(\nabla \times \vec{A}_2 \right)}{\mu_0} \right) \right\} \quad , \tag{2-8}$$

with A_z, $\vec{F}$, and ψ for the anisotropic medium given by

$$A_z = \frac{\mu_0 \gamma}{4j\sqrt{\mu_{xx} \mu_{yy}}} \int_C J_z(\vec{\rho}') H_0^{(2)}(k_a R_m) ds' \tag{2-9}$$

$$\vec{F} = \frac{\varepsilon_0 \varepsilon_z \gamma}{4j\sqrt{\mu_{xx} \mu_{yy}}} \int_C [\mu_2]^{-1} \cdot \vec{M}(\vec{\rho}') H_0^{(2)}(k_a R_m) ds' \tag{2-10}$$

$$\psi = \frac{1}{4j\mu_0 \sqrt{\mu_{xx} \mu_{yy}}} \int_C \rho_m(\vec{\rho}') H_0^{(2)}(k_a R_m) ds' \tag{2-11}$$

$$R_m = \sqrt{\frac{(x-x')^2}{\mu_{xx}} + \frac{(y-y')^2}{\mu_{yy}}} \quad , \tag{2-12}$$

where J_z, $\bar{M}$, and ρ_m are the equivalent electric and magnetic currents flowing on the surface of the scatterer and magnetic charge density, respectively. The magnetic charge density that acts as a source for ρ_m is related to the magnetic current density $\bar{M}$ by the continuity equation

$$\nabla \cdot \bar{M} = -j\omega\rho_m \quad . \tag{2-13}$$

Notice that equations (2-8) to (2-12) contain expressions for the potentials in the anisotropic region. These same equations can also be used to find the corresponding expressions for the potentials in the isotropic region by setting $\varepsilon_{zz} = \varepsilon_1$, $\mu_{xx} = \mu_{yy} = \mu_1$, and $\mu_{xy} = \mu_{yx} = 0$. At this point, equations (2-3) and (2-4) or (2-8) represent the desired combined field surface integral equation set required to analyze *TM* scattering.

The *TM*-polarized incident field in the scattering studies is assumed to be a plane wave whose electric and magnetic field components are given by

$$\bar{E}^i = \hat{z}E_0 e^{-j\bar{k}\cdot\bar{\rho}} \tag{2-14}$$

and

$$\bar{H}^i = \frac{\hat{k}^i \times \hat{z}E_0 e^{-j\bar{k}\cdot\bar{\rho}}}{\eta} \quad , \tag{2-15}$$

where η and k are the intrinsic impedance and propagation constant of Region 1, respectively. The corresponding RCS can be computed once the equivalent surface currents have been determined. The z-component of the scattered E-field is calculated from

$$E_z^s(\bar{\rho}) = \frac{-k\eta}{4}\int_C J_z(\bar{\rho}')H_0^{(2)}(kR)ds' + \frac{k}{4j}\int_C M_z(\bar{\rho}')\left(\hat{n}'\cdot\hat{R}\right)H_1^{(2)}(kR)ds' \tag{2-16}$$

by taking the large argument expansions for the Hankel functions. In the above equation $\hat{n}'$ and $\hat{R}$ are defined by

$$\hat{n}' = \hat{x}\cos\phi' + \hat{y}'\sin\phi' \tag{2-17}$$

$$\hat{R} = \frac{\vec{\rho} - \vec{\rho}'}{|\vec{\rho} - \vec{\rho}'|} \tag{2-18}$$

with ϕ' being the angle that the unit normal makes with the x-axis at the point of integration on the contour, and where $\vec{\rho}$ corresponds to the direction of far-field observation. Finally, the RCS can be computed from the following relation

$$\sigma \equiv \lim_{\rho\to\infty}\left(2\pi\rho\left|\frac{E_z^s}{E_z^i}\right|^2\right) , \tag{2-19}$$

with E_z obtained from equation (2-16).

2.2 Formulation of Radiation Problems

To illustrate the application of surface integral equations to radiation problems, the analysis of the anisotropic shell (or single-layer radome) illuminated by a line source placed inside it will be undertaken. Figure 2-2 shows the geometry under consideration which can be used to examine properties of single-layer two-dimensional anisotropic radomes. Although such structures are just idealized versions of the actual radome, a significant amount of information about the influence of anisotropy on *EM* fields radiating through a material layer having such properties can still be obtained.

In general, the excitation to the radome could be delivered in the form of an external plane wave or from an internally placed line source. For the plane wave incidence, the formulation of the scattering problem would proceed in the same way as for the bulk object considered in Section 2.1. However, the presence of an additional boundary would require for the combined field surface integral equations (CFSIEs) to also be obtained at the newly introduced boundary (Beker et al., 1990). Since the scattering problem for the

radome is similar to the radiation problem, at least in its integral equation formulation, the surface integral equations will only be provided for the latter case.

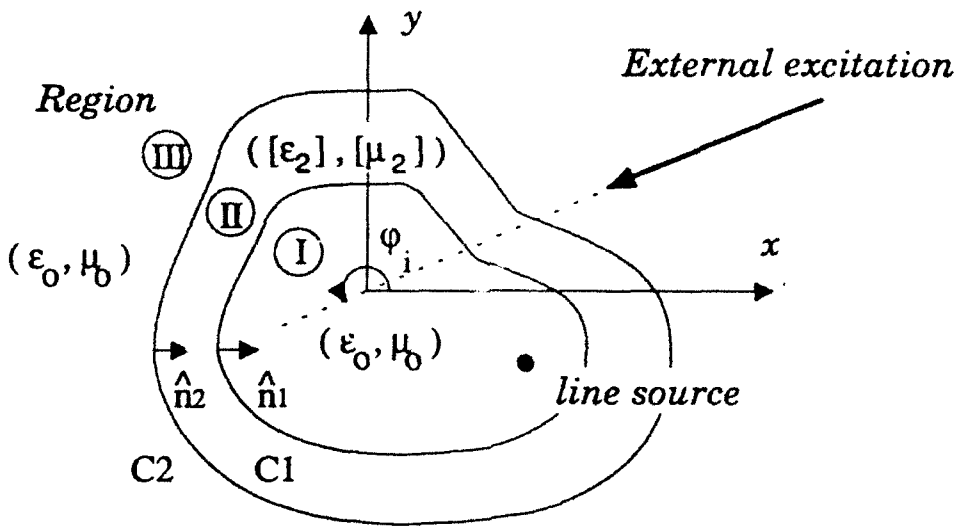

Figure 2-2: A two-dimensional anisotropic radome.

The boundary conditions (B.C.s) on the tangential field components at boundary contours C_1 and C_2 lead to the following set of CFSIEs for the radome shown in Fig. 2-2. At the inner contour, matching E- and H-fields yields:

$$-E_{z_1}^{i} = -j\omega(A_{z1} + A_{z2}) - \hat{z}\cdot\left(\frac{\nabla\times\vec{F}_1}{\varepsilon_0\varepsilon_1} + \frac{[\varepsilon_2]^{-1}\cdot(\nabla\times\vec{F}_2)}{\varepsilon_0}\right) \tag{2-20}$$

$$-\hat{n}\times\vec{H}_1^{i} = -\hat{n}\times\left\{j\omega\left(\vec{F}_1+\vec{F}_2\right)+\nabla(\psi_1+\psi_2)-\left(\frac{\nabla\times\vec{A}_1}{\mu_0\mu_1}+\frac{[\mu_2]^{-1}\cdot(\nabla\times\vec{A}_2)}{\mu_0}\right)\right\}, \tag{2-21}$$

and then at the outer contour the B.C.s result in

$$0 = -j\omega(A_{z3} + A_{z2}) - \hat{z}\cdot\left(\frac{\nabla\times\vec{F}_3}{\varepsilon_0\varepsilon_3} + \frac{[\varepsilon_2]^{-1}\cdot(\nabla\times\vec{F}_2)}{\varepsilon_0}\right) \tag{2-22}$$

$$0 = -\hat{n} \times \left\{ j\omega\left(\vec{F}_3 + \vec{F}_2\right) + \nabla\left(\psi_3 + \psi_2\right) - \left(\frac{\nabla \times \vec{A}_3}{\mu_0 \mu_3} + \frac{\left[\mu_2\right]^{-1} \cdot \left(\nabla \times \vec{A}_2\right)}{\mu_0} \right) \right\} \quad , \tag{2-23}$$

where subscript 3 corresponds to Region 3, which for this problem is air. Expressions for the vector and scalar potentials are same as those given earlier in Section 2.1, and incident fields are those of the line source.

For this problem, the *TM*-polarized line source has E and H fields that are given by the following expressions (Balanis, 1989)

$$\vec{E}^i = -\hat{z}\frac{k\eta}{4} I_e f(\rho,\varphi) H_0^{(2)}\left(k\left|\vec{\rho} - \vec{\rho}'\right|\right) \tag{2-24}$$

and

$$\vec{H}^i = \frac{-\nabla \times \vec{E}^i}{j\omega\mu} \quad , \tag{2-25}$$

where I_e and $f(\rho,\varphi)$ are the line source current and taper pattern function, respectively.

2.3 Method of Moments (MOM) Numerical Solution

The surface integral equations, whether they are cast in terms of vector potentials only or they are stated in terms of mixed potentials, can be solved numerically by the Method of Moments (Harrington, 1968). The only difference between these two formulations from the stand-point of the numerical implementation is the complexity of integrals that are involved in filling of the system matrix. In the Galerkin procedure, both expansion and testing functions are taken to be of the same type, and for all results appearing in this report they were chosen to be the unit pulse functions.

The unknown equivalent electric and magnetic surface currents $\left(J_s, M_s\right)$ are first expanded as weighted sums of pulse basis functions

$$J_z(\vec{\rho}') = \sum_{n=1}^{N} p_n^J(\vec{\rho}_n') J_{zn} \tag{2-26}$$

$$M_z(\vec{\rho}') = \sum_{n=N+1}^{2N} p_n^M(\vec{\rho}_n') M_{zn} \quad . \tag{2-27}$$

These same unit pulse functions can also serve as the testing functions for E- and H-field equations

$$t^E(\vec{\rho}) = \sum_{m=1}^{M} p_m^J(\vec{\rho}_m) \tag{2-28}$$

$$t^H(\vec{\rho}) = \sum_{m=M+1}^{2M} p_m^M(\vec{\rho}_m) \quad . \tag{2-29}$$

Since the scatterer can have surface discontinuities, some components of the electric and magnetic fields can be singular at these points, whether the objects are conducting (Jackson, 1975), isotropic (Bach Andersen et al., 1978; Van Bladel, 1985; and Marx, 1990), or anisotropic (Beker, August 1991). For *TM* scattering, this means that the tangential H-field (or J_z) is singular at the surface discontinuity. On the other hand, the tangential component of the electric field (or M_z) is continuous at that same location.

To properly represent such field behavior, the standard procedure is to stagger the equivalent surface current pulse functions as shown in Fig. 2-1. This form of expansion builds in the proper field behavior numerically, thus avoiding sampling of singular magnetic fields at sharp corners or numerically violating charge conservation of the magnetic charge density.

Once expansion and testing are completed, CFSIEs are converted to a set of linear matrix equations, which for the bulk scatterer with a single boundary, take on the following form:

$$\begin{bmatrix} [Z^E_{mn}] & [Y^E_{mn}] \\ [Z^H_{mn}] & [Y^H_{mn}] \end{bmatrix} \begin{bmatrix} [J_{sn}] \\ [M_{sn}] \end{bmatrix} = \begin{bmatrix} [E^i_{sm}] \\ [H^i_{sm}] \end{bmatrix} \quad (2\text{-}30)$$

The individual submatrix elements of the above matrix system for the vector potential formulation (equations 2-3 and 2-4) are explicitly defined elsewhere (Beker et al., 1989) and, therefore, are not repeated here.

Although for anisotropic scatterers the mixed potential formulation (equations 2-3 and 2-8) has been implemented numerically (Beker et al., 1990), explicit expressions for the matrix elements of equation (2-30) do not appear in print. However, the MOM approach is very similar to that used in CFSIEs for isotropic scatterers and for this reason is omitted from this report. However, an interested reader is referred to (Umashankar, et al., 1984), among other references, for details on the numerical procedure required to reduce the CFSIEs to a matrix form for isotropic scatterers.

Section 3

MOM NUMERICAL EXAMPLES

This Section summarizes numerical results obtained for anisotropic scatterers. These include solid circular lossless cylinders, thin lossy plates, coated metallic circular cylinders, and circular shells. The combined field integral equations, presented in the previous Section, were solved using the Method of Moments. The MOM codes, developed at the University of South Carolina, were written in FORTRAN. All data were generated on an IBM-compatible 486-50 MHz PC, using version 4.01 of Lahey Fortran Compiler. The largest matrix size of 480 x 480 was required for anisotropic shells to account for the unknowns on both its internal and external contours. The solution time of approximately 10 minutes was needed to obtain equivalent surface currents and bistatic RCS or radiation pattern for a single frequency point.

3.1 Plane Wave Scattering From Circular Cylinders

A circular anisotropic cylinder, illuminated by a normally incident *TE* polarized plane wave, is shown in Fig. 3-1. The frequency of the incident field is assumed to be 300 MHz, and the electrical size of the object is $k_0 a = \pi/2$. Three different sets of anisotropic medium parameters were chosen to illustrate the differences in scattering properties of such cylinders when compared to their isotropic counterparts. The MOM code used in computations was validated in earlier studies against the plane wave expansion method (Fig. 3 of Beker, 1989). The number of unknowns for all circular cylinder studies was 120 for each equivalent surface current, resulting in the total of 240 unknowns.

As mentioned above, three different sets of the permittivity tensor elements were considered: $(\varepsilon_{xx} = 2, \varepsilon_{yy} = 4)$, $(\varepsilon_{xx} = 4, \varepsilon_{yy} = 2)$, and $(\varepsilon_{xx} = 2, \varepsilon_{yy} = 4, \varepsilon_{xy} = -\varepsilon_{yx} = 2)$ — and in all cases $\mu_{zz} = 2$. Notice from the integral equations presented in Section 2 that the formulation for the *TE* polarization involves only transverse elements of [ε] and only the axial element of [μ]. According to duality (Beker et al., 1990), scattering by *TM* polarized excitation will only involve transverse elements of [μ] and the axial element of [ε]. This

means that under *TM* excitation, the cylinder will look isotropic to the incident field, if the material is nonmagnetic.

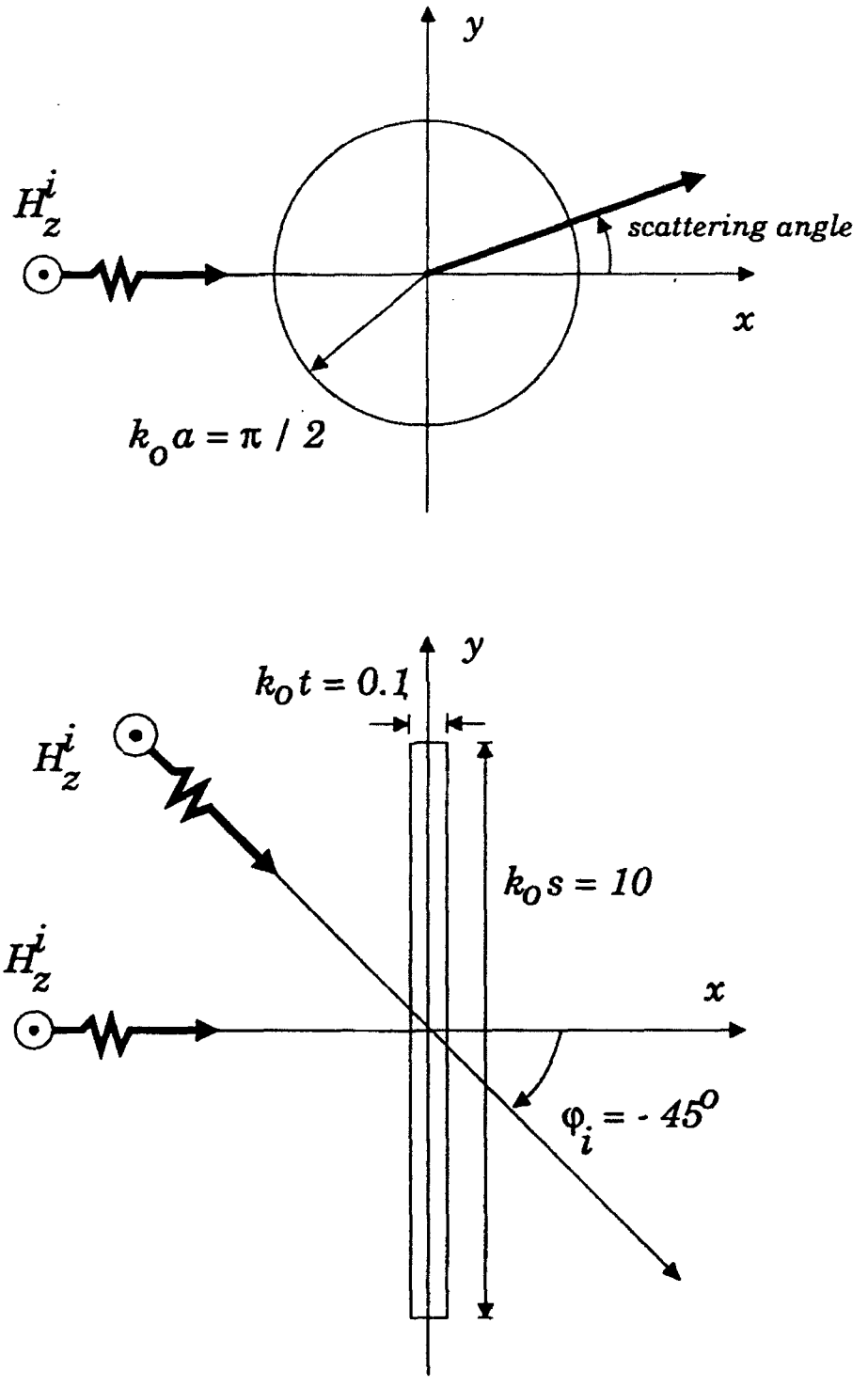

Figure 3-1. Geometry of a circular cylinder and a thin cylindrical plate.

Figures 3-2 through 3-5 show comparisons between the scattering properties of isotropic and anisotropic circular cylinders. In this case, the relative permeability of the isotropic cylinder is $\mu_r = 2$ and the axial element of $[\mu]$ for the anisotropic scatterer is $\mu_{zz} = 2$. The intent of these numerical studies is to illustrate how the scattering properties of highly symmetric objects such as circular cylinders can be affected by anisotropy of the material. The RCS of circular anisotropic cylinders whose permittivity tensors are diagonal, namely $(\varepsilon_{xx} = 2, \varepsilon_{yy} = 4)$ and $(\varepsilon_{xx} = 4, \varepsilon_{yy} = 2)$, are plotted in Fig. 3-2 along with the RCS of the isotropic scatterer whose permittivity is $\varepsilon_r = 2$. As can be seen, the RCS of the three cylinders differs considerably, especially in the angular range of 90 to 180 degrees. This graph also contains a very interesting feature. More specifically, when the scattering angle becomes 90 or 270 degrees, the RCS of *all* three cylinders is *same*!

In the next example, the scattering cross section of the isotropic cylinder with $\varepsilon_r = 4$ and $\mu_r = 2$ is compared to the same anisotropic cylinders that were mentioned above. Figure 3-3 displays the corresponding RCS curves, indicating the degree of dissimilarity between them. Notice that in this case, the RCS level of anisotropic cylinder with $(\varepsilon_{xx} = 2, \varepsilon_{yy} = 4)$ (case (b)) is somewhere between the RCS of the other two scatterers.

Final examples of RCS calculation for circular cylinders are shown in Figs. 3-4 and 3-5. They emphasize the changes in scattering characteristics of symmetric objects that are associated with the addition of the off-diagonal elements to the permittivity tensor. The most evident on the RCS as $\varepsilon_{xy} = -\varepsilon_{yx} = 2$ are introduced, is a dramatic reduction in the field level scattered from the cylinder. In fact, the reduction is by more than 10 dB, as compared to both isotropic or anisotropic scatterers. This is obviously attributed to the presence of ε_{xy} and ε_{yx}. The net effect of these elements is to reradiate the scattered field in different directions, rather that focusing the energy in one direction only.

The secondary effect on the RCS due to introduction of ε_{xy} and ε_{yx} is the destruction of the symmetry of the scattered field about the direction of incidence. This indicates that even though the geometry of the object is highly symmetric, the shape of the scattered field pattern can be controlled independently by its material parameters.

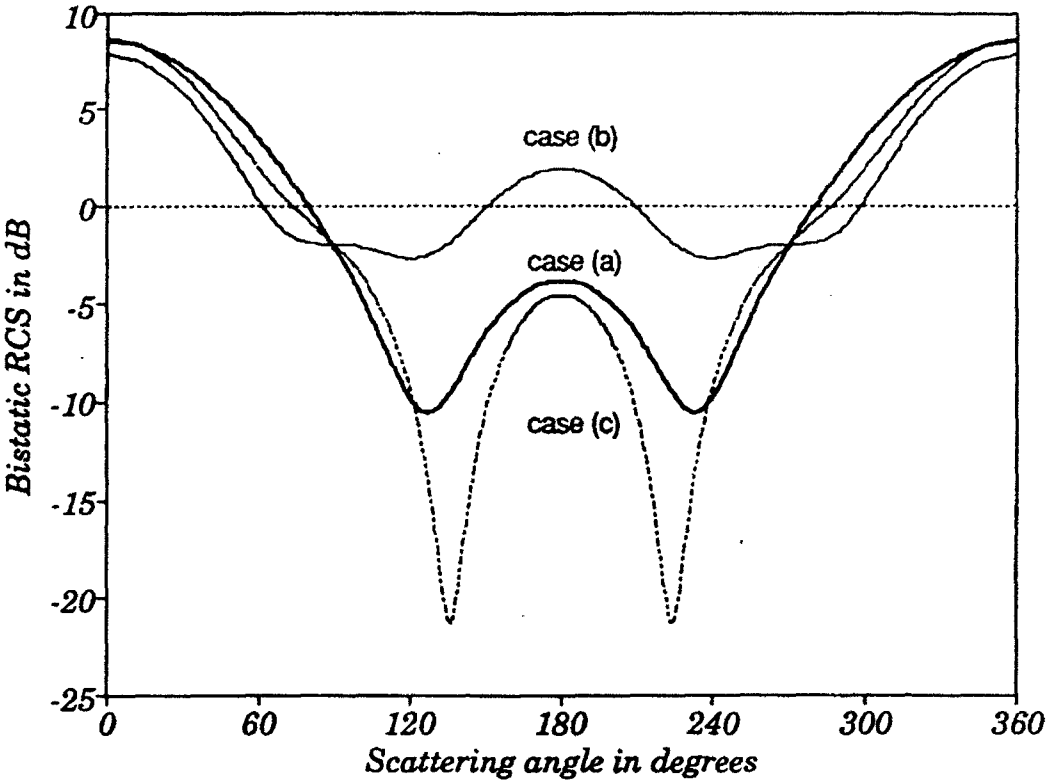

Figure 3-2. RCS Comparison for isotropic and anisotropic circular cylin ers. Case (a) $\varepsilon_r = 2$, $\mu_r = 2$, Case (b) $\varepsilon_{xx} = 2, \varepsilon_{yy} = 4; \mu_z = 2$, Case (c) $\varepsilon_{xx} = 4, \varepsilon_{yy} = 2; \mu_z = 2$.

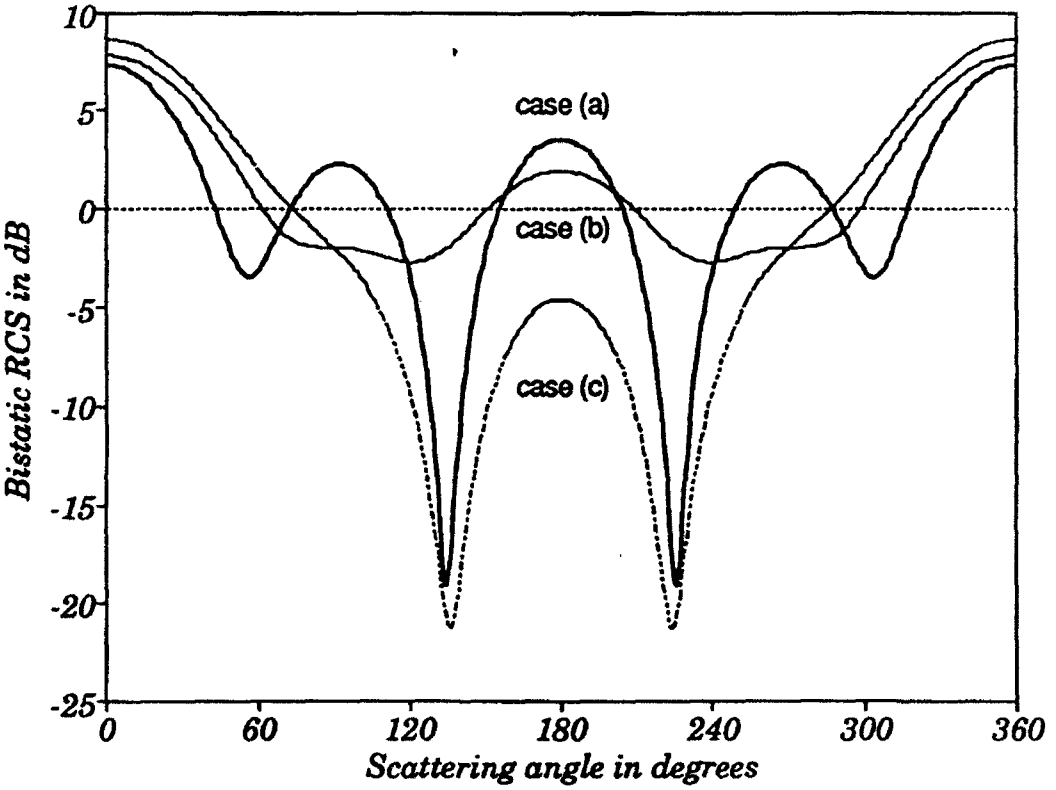

Figure 3-3. RCS Comparison for isotropic and anisotropic circular cylinders. Case (a) $\varepsilon_r = 4$, $\mu_r = 4$, Case (b) $\varepsilon_{xx} = 2, \varepsilon_{yy} = 4; \mu_z = 2$, Case (c) $\varepsilon_{xx} = 4, \varepsilon_{yy} = 2; \mu_z = 2$.

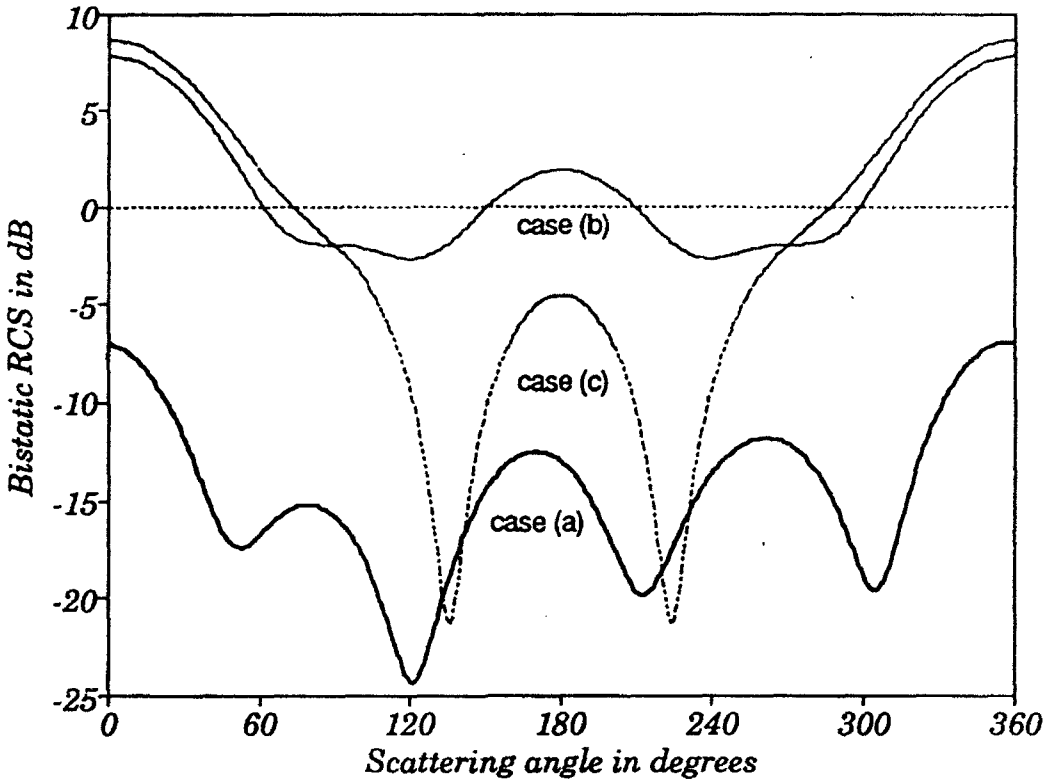

Figure 3-4. RCS Comparison for three different anisotropic circular cylinders. Cases (a), (b), and (c): $(\varepsilon_{xx}=2,\varepsilon_{yy}=4,\varepsilon_{xy}=-\varepsilon_{yx}=2;\mu_{z}=2)$, $(\varepsilon_{xx}=2,\varepsilon_{yy}=4;\mu_{z}=2)$, $(\varepsilon_{xx}=4,\varepsilon_{yy}=2;\mu_{z}=2)$.

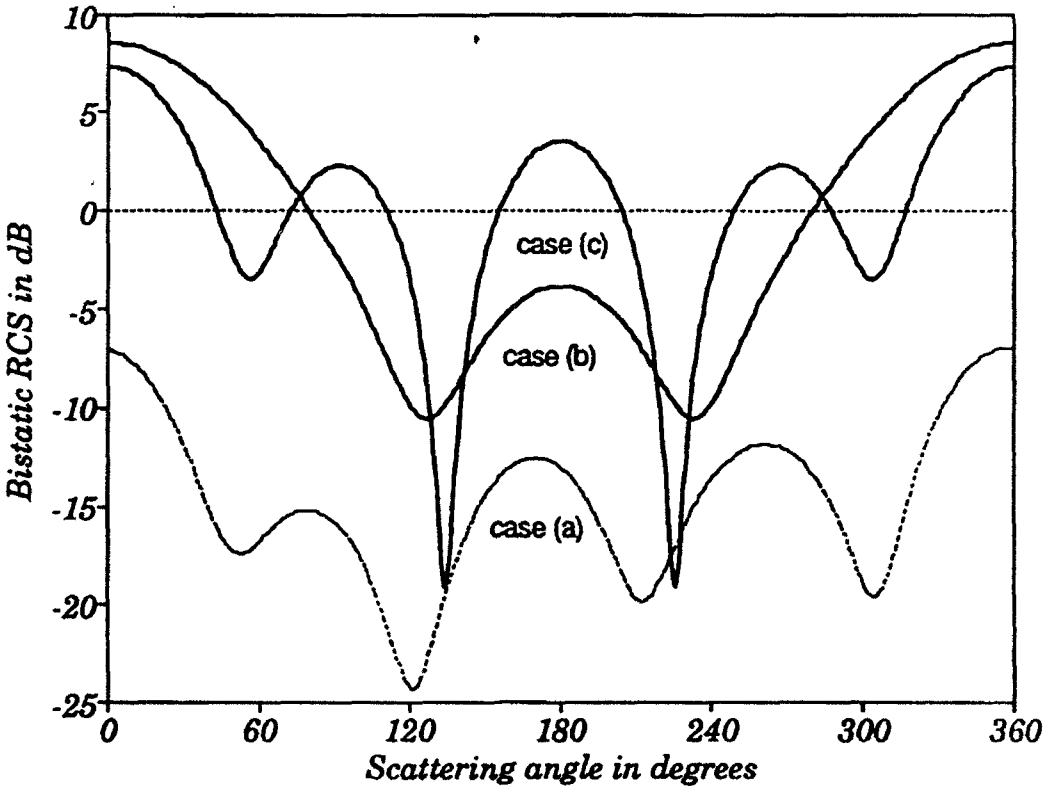

Figure 3-5. RCS Comparison for three different circular cylinders. Cases (a), (b), and (c): $(\varepsilon_{xx}=2,\varepsilon_{yy}=4,\varepsilon_{xy}=-\varepsilon_{yx}=2;\mu_{z}=2)$, $(\varepsilon_{r}=2,\mu_{r}=2)$, $(\varepsilon_{r}=4,\mu_{r}=2)$.

3.2 Plane Wave Scattering From Cylindrical Plates

To examine effects of material anisotropy on objects with less symmetric geometries than that of a circular cylinder, the scattering properties of a thin plate were also computed. The anisotropic plate, shown in Fig. 3-2, is lossless and is characterized by three sets of material parameters, namely $(\varepsilon_{xx}=2,\varepsilon_{yy}=4)$, $(\varepsilon_{xx}=4,\varepsilon_{yy}=2)$, and $(\varepsilon_{xx}=2,\varepsilon_{yy}=4,\varepsilon_{xy}=-\varepsilon_{yx}=2)$ or cases (a), (b), and (c), respectively. For all these plates the zz-element of permeability tensor was assumed to be equal to 2. The excitation to the scatterer is a TE-polarized plane wave whose frequency is 300 MHz. Two directions of incidence were considered: one broadside, the second inclined 45 degrees with respect to the y-axis.

The radar scattering cross-sections for both angles of incidence are displayed in Figs. 3-6 and 3-7. As shown in Fig. 3-6, for broadside incidence, the RCS patterns of plates with different diagonal permittivity tensors differ significantly. This is particularly evident in the backscattering direction ($\varphi_s=180°$). At this angle, the RCS corresponding to case (b) is nearly 30 dB lower than the calculated RCS for case (a). This result is attributed to the incident field, which at this angle has a y-component only and senses a higher value of ε_{yy} in case (a) than in case (b), that is, $\varepsilon_{yy}=4$ rather than $\varepsilon_{yy}=2$.

Note that for the plate, the addition of the off-diagonal elements to [ε] has an opposite effect on the RCS as it did for the circular cylinder. Specifically, introduction of $\varepsilon_{xy}=-\varepsilon_{yx}=2$ seems to raise the RCS level in both forward and backscattering directions (case (c) in Fig. 3-6), whereas for the circular cylinder (Fig. 3-4) the opposite was true. One possible explanation of such behavior is that the plate is electrically thin and its scattering characteristics are governed primarily by ε_{yy}. In fact, as can be seen from Fig. 3-6, curves (a) and (c) are not that different from one another, except the asymmetry and somewhat higher RCS levels for case (c).

As the direction of incidence is skewed, the scattered field from the plate changes considerably. Under such conditions the incident field, which now has both x- and y-components, senses every element of [ε] equally. Consequently, as illustrated in Fig. 3-7, there are no drastic differences in the RCS of all three plates. Observe that similarity between cases (b) and (c) is still in evidence, despite the change in angle of incidence.

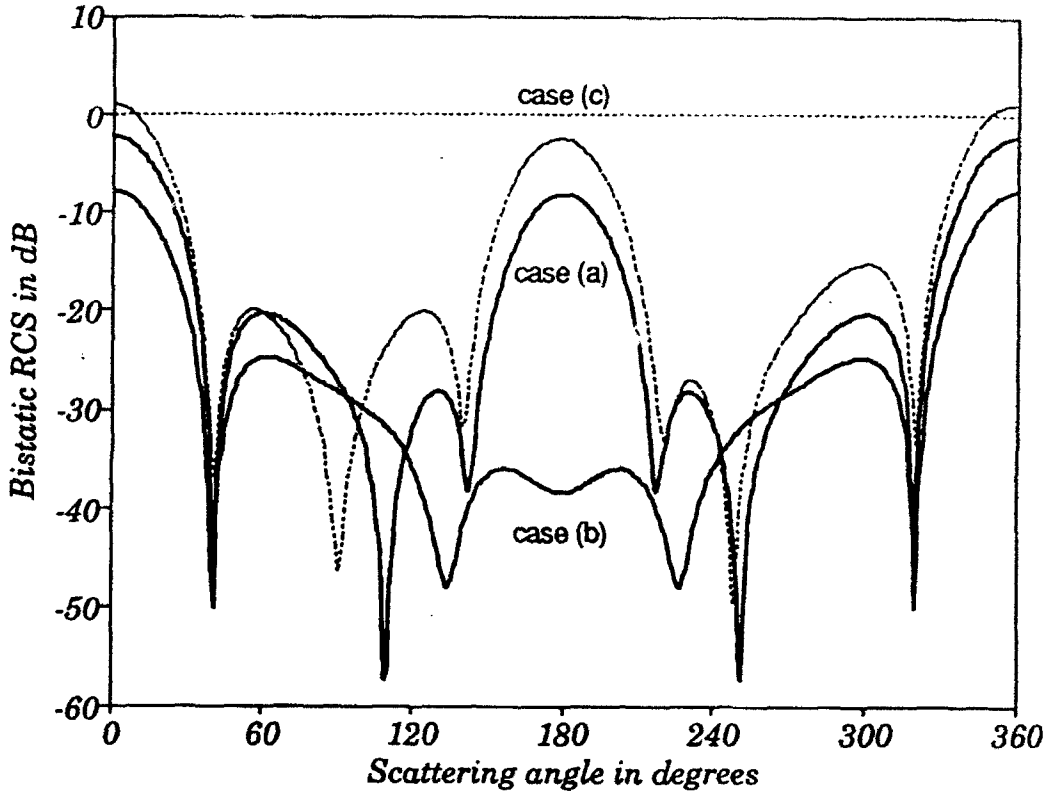

Figure 3-6. RCS Comparison for three different anisotropic cylindrical plates, $\varphi_i = 0^0$. Case (a) $\varepsilon_{xx} = 2, \varepsilon_{yy} = 4$, Case (b) $\varepsilon_{xx} = 4, \varepsilon_{yy} = 2$, Case (c) $\varepsilon_{xx} = 2, \varepsilon_{yy} = 4, \varepsilon_{xy} = -\varepsilon_{yx} = 2$.

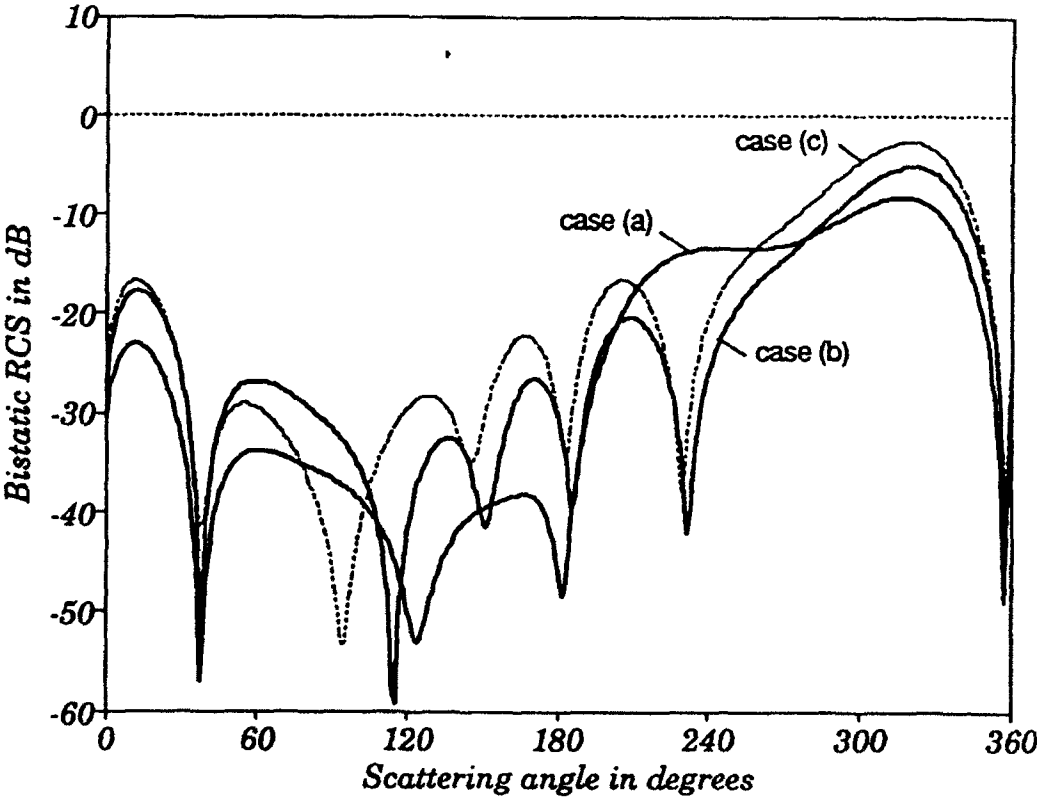

Figure 3-7. RCS Comparison for three different anisotropic cylindrical plates, $\varphi_i = -45^0$. Case (a) $\varepsilon_{xx} = 2, \varepsilon_{yy} = 4$, Case (b) $\varepsilon_{xx} = 4, \varepsilon_{yy} = 2$, Case (c) $\varepsilon_{xx} = 2, \varepsilon_{yy} = 4, \varepsilon_{xy} = -\varepsilon_{yx} = 2$.

In earlier examples, the anisotropic medium was assumed to be characterized by individual tensor elements whose numerical values were quite different from one another. For the following examples, the medium parameters correspond to those of actual composite media that were determined from the measurements. Numerical results for the RCS were obtained for an E-glass plate having ε_{xx} and ε_{yy} values ranging from $5-j0.1$ to $5-j0.125$ and from $4.5-j0.09$ to $4.5-j0.1125$, respectively. Since E-glass is non-magnetic, both μ_x and μ_r in the numerical simulations were set equal to 1. The excitation to the plate is still in a form of a *TE*-polarized plane wave with the frequency of 300 MHz, striking it broadside.

Figures 3-8 and 3-9 show the comparison between the RCS patterns of lossy isotropic and anisotropic plates. The isotropic scatterer, in this case, is characterized by a complex dielectric constant $\varepsilon_r = 5-j0.125$. It is apparent that the small degree of anisotropy in E-glass is responsible for lowering the RCS level by 1 dB over the entire range of the scattering angle. Once again, the scattering properties of the cylindrical plate seem to be governed by the *yy*-element of the permittivity tensor. Since both the real and imaginary parts of ε_{yy} are smaller than the real and imaginary parts of ε_r, both forward and backscattering power levels of the anisotropic plates are lower than those of their isotropic counterpart, as was expected. This behavior emphasizes the fact that even low anisotropy can affect the response of the scattering object to the incident field, especially to its polarization.

3.3 Plane Wave Scattering From Coated Circular Cylinders

The data, shown in Figs. 3-11 through 3-14, concentrate exclusively on the effects of anisotropy on the RCS of conducting cylinders that are coated with a single layer of lossless anisotropic material. The normalized radius of the conducting core is $k_0 b = 1$, and the radius of the coating layer is $k_0 a = 2$ (see Fig. 3-10). As in all the previous cases, the coated scatterers are also excited with a *TE*-polarized plane wave whose frequency is 300 MHz, and which is incident at $\varphi_i = 0^o$.

Results in Figs. 3-11 and 3-12 convey the differences in RCS plots of lossless anisotropic ($\varepsilon_{xx} = 5, \varepsilon_{yy} = 4.5$) and isotropic coatings with ε_r being 4.5 or 5. At the same time, the data displayed in Figs. 3-13 and 3-14 show the comparison of RCS patterns corresponding to the anisotropic coating whose diagonal elements of [ε] are

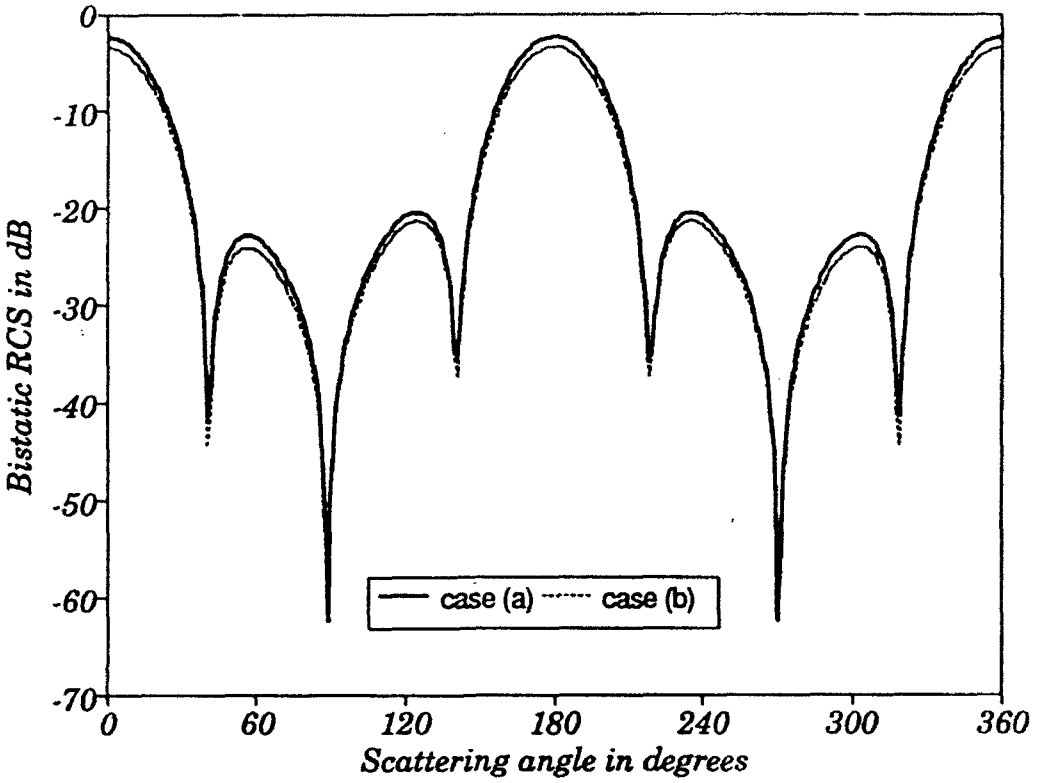

Figure 3-8. RCS Comparison for isotropic and anisotropic cylindrical plates, $\varphi_i = 0^0$. Case (a) $\varepsilon = 5 - j0.125$, Case (b) $\varepsilon_{xx} = 5 - j0.125, \varepsilon_{yy} = 4.5 - j0.09$.

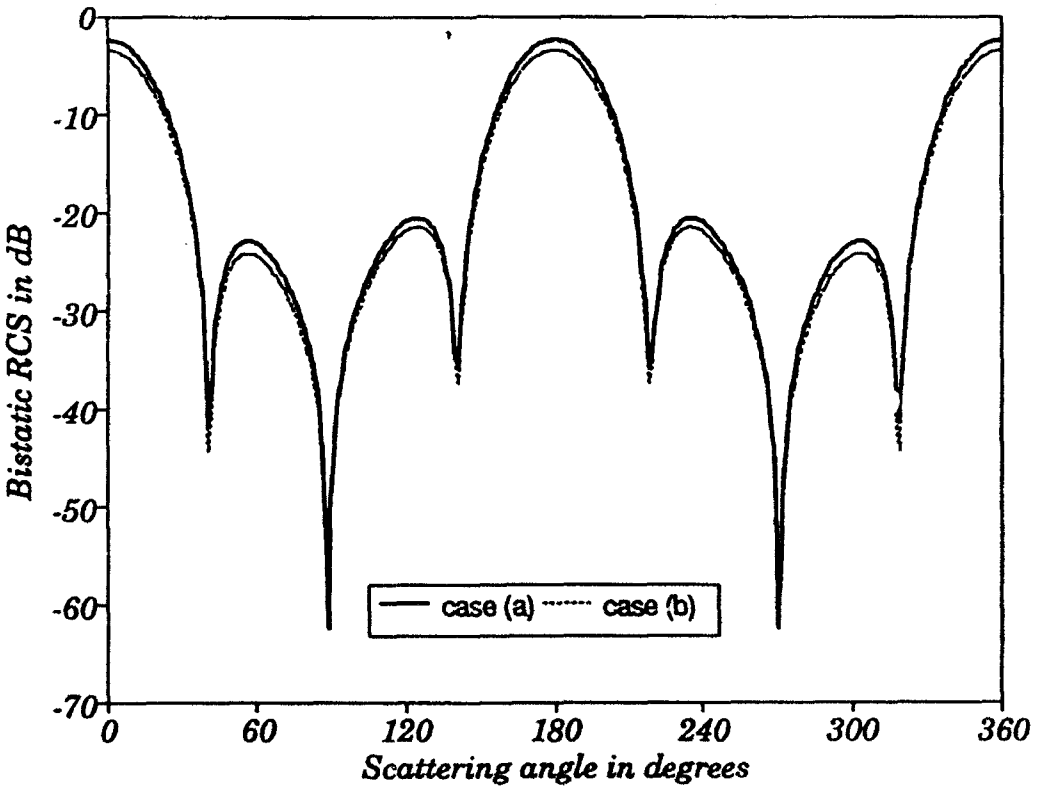

Figure 3-9. RCS Comparison for isotropic and anisotropic cylindrical plates, $\varphi_i = 0^0$. Case (a) $\varepsilon = 5 - j0.125$, Case (b) $\varepsilon_{xx} = 5 - j0.1, \varepsilon_{yy} = 4.5 - j0.1125$.

($\varepsilon_{xx} = 4.5, \varepsilon_{yy} = 5$) and those of the isotropic coating layers whose ε_r is 4.5 or 5. The scattered field levels, for the most part, follow the expected trends, with the RCS being higher for anisotropic coatings whose ε_{yy} is greater than ε_r, and lower when ε_{yy} is less than ε_r.

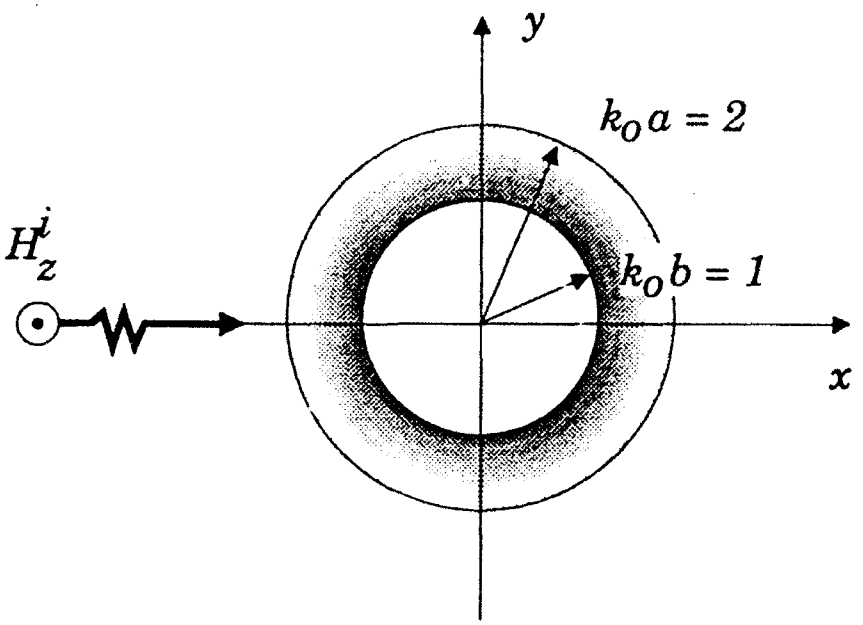

Figure 3-10. Geometry of a coated conducting circular cylinder.

In addition to the expected behavior, numerical results for coated objects have other features. For example, there are pattern cross-overs and wide angular sectors where the RCS of isotropic as well as anisotropic scatterers are identical. The greatest discrepancies in the RCS plots, however, are confined to forward and backward scattering directions, as well as to the null locations. Such scattering behavior is not the same as was seen earlier for solid isotropic and anisotropic circular cylinders (Figs. 3-2 to 3-5).

Recall that for the solid circular scatterers, there was no correlation between the RCS of any anisotropic cylinders with the RCS of any isotropic cylinders. In fact, the two sets of patterns had very little in common. The same can no longer be said for loaded circular cylinders. This is most evident in Figs. 3-13, wherein there is hardly any difference between the displayed RCS patterns. This is a direct consequence of having a relatively large conducting core that both anisotropically and isotropically loaded scatterers have in common.

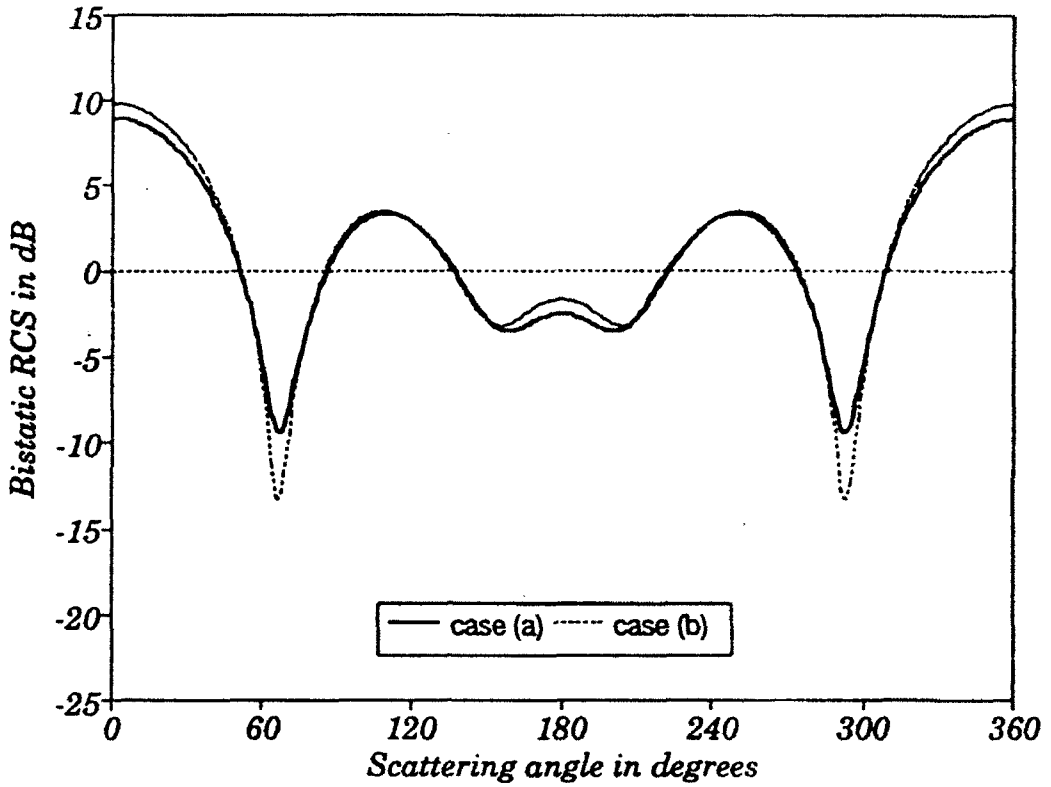

Figure 3-11. RCS of isotropic and anisotropic loaded circular cylinders. Case (a) $\varepsilon_r = 4.5$, Case (b) $\varepsilon_{xx} = 5, \varepsilon_{yy} = 4.5$,

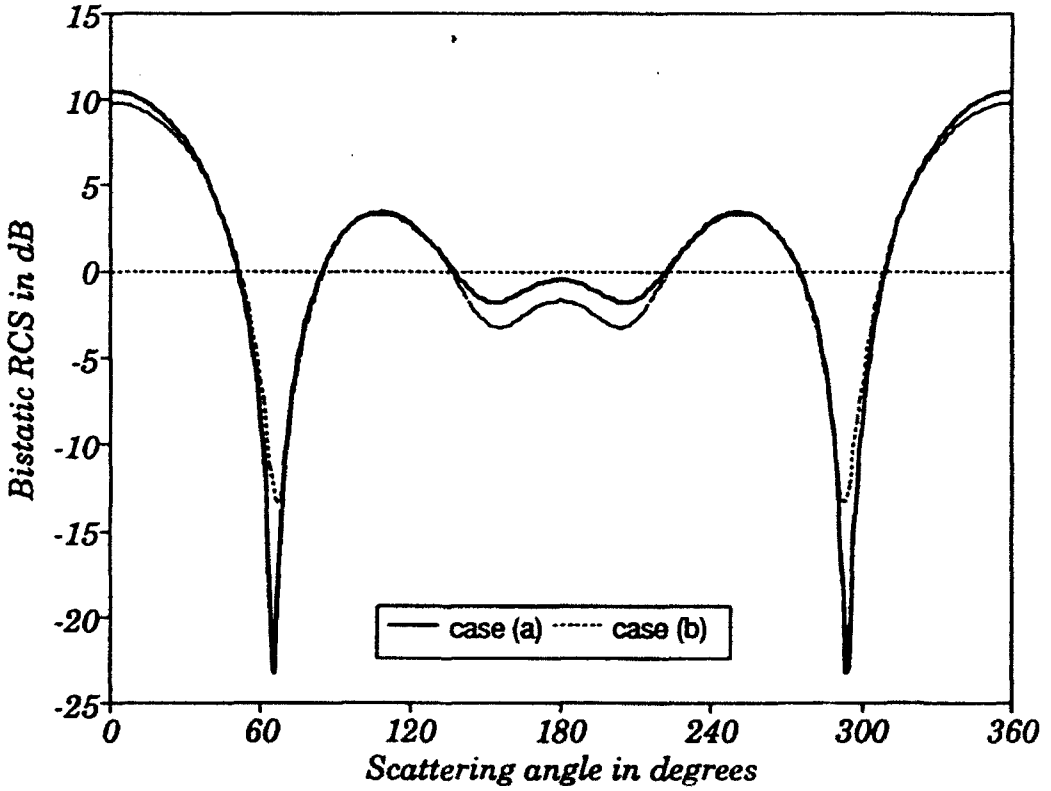

Figure 3-12. RCS of isotropic and anisotropic loaded circular cylinders. Case (a) $\varepsilon_r = 5$, Case (b) $\varepsilon_{xx} = 5, \varepsilon_{yy} = 4.5$.

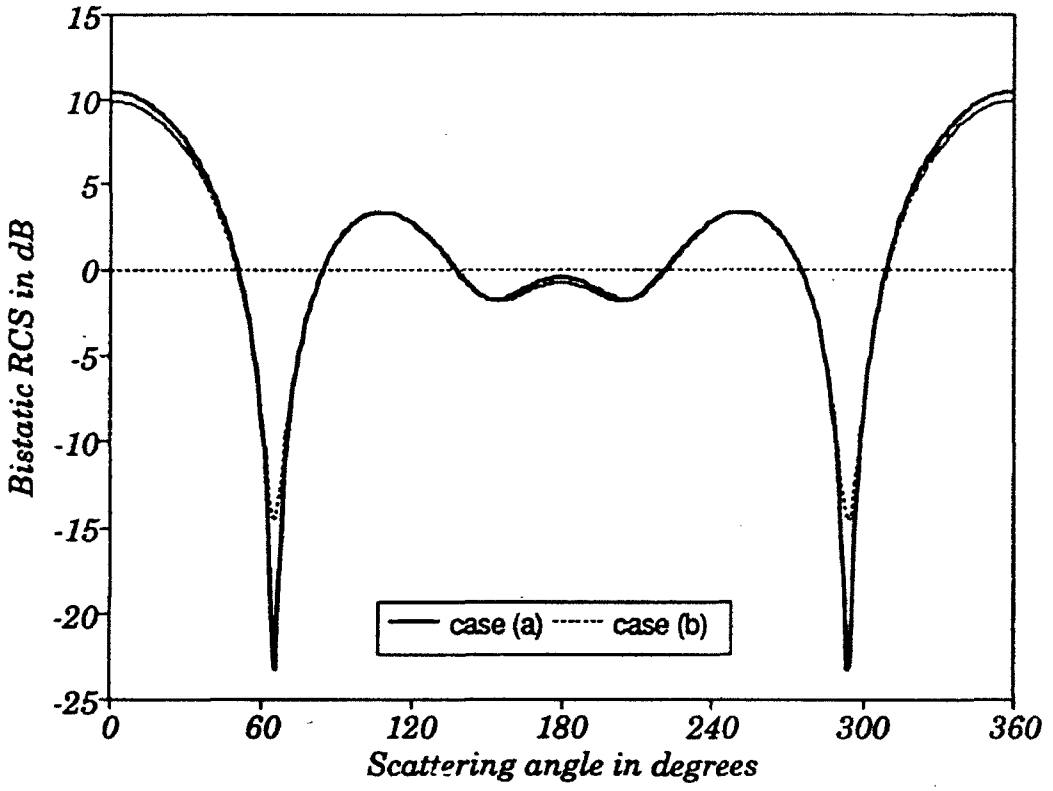

Figure 3-13. RCS of isotropic and anisotropic loaded circular cylinders. Case (a) $\epsilon_r = 4.5$, Case (b) $\epsilon_{xx} = 4.5, \epsilon_{yy} = 5$.

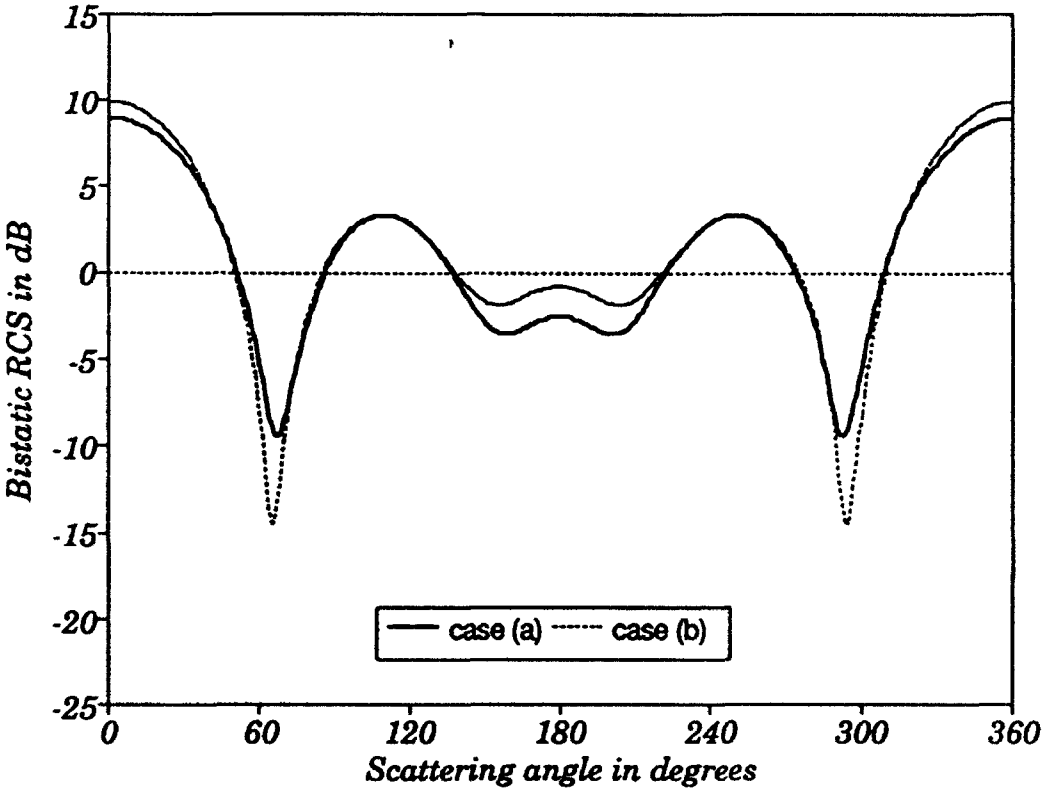

Figure 3-14. RCS of isotropic and anisotropic loaded circular cylinders. Case (a) $\epsilon_r = 5$, Case (b) $\epsilon_{xx} = 4.5, \epsilon_{yy} = 5$.

3.4 Radiation From a Line Source Inside a Circular Shell

The effects of material anisotropy on the radiation characteristics of a uniform line source placed inside a circular shell centered at the coordinate origin are now presented. The motivating factor behind the choice of a circular geometry for the radiation studies was the need to emphasize effects of the material rather than the shape of the object on its radiation properties. The shell was assumed to be lossy, while its internal and external radii were chosen to be 0.1 and 0.125 meters. The *TE*-polarized source, whose frequency is 400 MHz, is located at the center and is assumed to be radiating uniformly in all directions.

Numerical results displayed in Fig. 3-15 correspond to power loss estimates as functions of the anisotropy in the conductivity of the material. The two curves that appear in this figure were calculated by varying one element of $[\sigma]$ while keeping the other one fixed. The real parts of ε_{xx} and ε_{yy} of the shell are 5 and 4.5, respectively. An estimate of the power loss due to dissipation of power in the material and due to reflection back into the core of the structure were calculated along the direction of the main beam, according to the following relation

$$\Delta P = \frac{\left|E_z^{rad}([\sigma]=0)\right|^2 - \left|E_z^{rad}([\sigma]\neq 0)\right|^2}{\left|E_z^{rad}([\sigma]=0)\right|^2} \quad .$$

Notice that the power loss in not the same for increasing loss tangent values in x- and y-direction. The loss is higher for changing values of σ_{xx} when compared to same changes in σ_{yy}. This behavior is rather surprising since the electric field of the *TE*-excitation senses both complex elements ε_{xx} and ε_{yy} almost equally.

Finally, the corresponding radiation pattern of a line source located inside the circular radome is shown in Fig. 3-16, which contains a very important feature. Despite the highly symmetric geometry and uniformity of the excitation, the calculated radiation pattern is *not uniform*! This is a direct consequence of material anisotropy, even though the actual difference between ε_{xx} and ε_{yy} is small. This added directivity to radiation pattern can be increased even further by selecting larger differences between the various tensor elements.

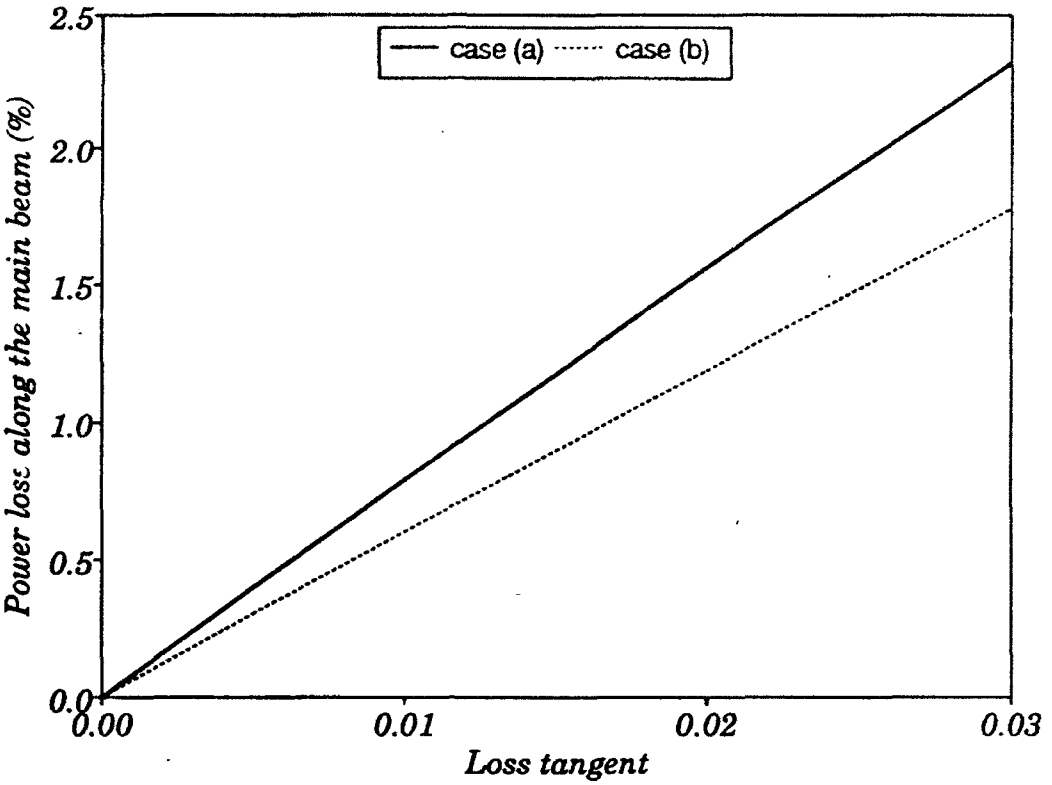

Figure 3-15. Power loss in the direction of the main beam vs. the loss tangent. Case (a) $\tan\delta_{xx}$, Case (b) $\tan\delta_{yy}$.

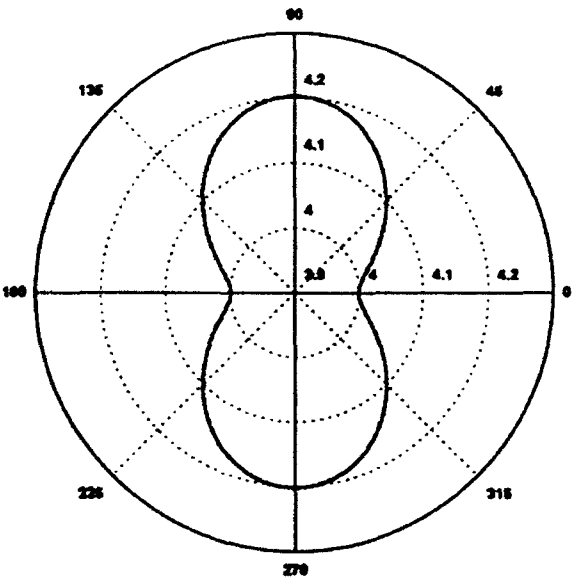

Figure 3-16. Radiation pattern of a uniform line source placed inside anisotropic shell.

Section 4

SUMMARY

In this report, combined-field surface integral equations were shown to be a viable tool for the analysis of electromagnetic field interaction with anisotropic materials. The method of moments solution to the CFSIEs was obtained and used to generate numerical results to illustrate effects of material anisotropy of scattering and radiation properties of arbitrarily shaped two-dimensional objects. Several canonical geometries such as solid and loaded circular cylinders as well as cylindrical plates were considered which can be used effectively to investigate EM properties of composite materials.

Numerical studies indicate that material anisotropy, no matter how small, can have a significant effect on the electromagnetic response of scatterers composed of such media. This is especially true of composite materials which are known to be anisotropic. The computed radar cross-sections of objects with highly symmetric geometries show that depending on the values of the tensor elements, their scattered fields can be changed considerably. Even asymmetry in the far-field pattern can be introduced with addition of the off-diagonal terms to the permittivity tensor. The asymmetry seems also to be associated with a significant reduction in the RCS resulting from redirection of the incident field by the constitutive properties of the material.

Additional studies show that when the scatterer is electrically thin and elongated at the same time, such as the plate, then its scattering response is largely controlled by a single tensor element that is most heavily exposed to the incident field. Under these conditions, the anisotropic scatterer behaves much like its isotropic counterpart having scalar permittivity equal to that of the dominant tensor element, which is most prominently sensed by the excitation. This implies that electrically thin objects are sensitive to the polarization of the incident field.

As opposed to bulk or solid objects, conducting objects that are coated with a thick layer of anisotropic material are less sensitive to its tensor characteristics or the polarization of the excitation. From the numerical results, it appears that the conducting

core lessens the effects of anisotropy by not allowing for the field to totally penetrate the composite structure.

The radiation studies reveal additional features of anisotropic material interaction with electromagnetic fields that are otherwise unobtainable with their isotropic counterparts. In the circular shell radome example, it was found that the radiation characteristics of a uniform line source, placed inside this radome, are affected by the anisotropic material properties of the radome. In particular, it was observed that directivity can be introduced to the radiation pattern by the presense of the anisotropy. This is a very important feature for it can be used to provide additional degrees of freedom to the design of shielding structures that are impossible to achieve with conventional isotropic materials.

In addition to introducing directivity to the radiation pattern, anisotropy can also affect the power loss of the radome. This power loss is defined as a fraction of power transmitted through a layer of lossy and lossless material, and hence is a sum of transmitted power reduction due to reflection and dissipation loss. If the conductivity of the material is also characterized by a tensor, then the level of power loss becomes dependent on the polarization of the excitation. It was found that a combination of factors such as the real and imaginary parts of the complex permittivity tensor produce different levels of power loss through the radome.

From the results presented in this report, it can be safely concluded that the effects of material anisotropy are not negligible in the investigation of their interaction with electromagnetic fields. They have to be taken into account in any numerical methods used to simulate EM response of structures with such material properties. Even a small degree of anisotropy can be important, especially in problems involving high power electromagnetic fields.

Section 5

REFERENCES

Bach Andersen, J. and V. V. Soloduhkov. 1978. "Field behavior Near a Dielectric Wedge," *IEEE Trans. Antennas Prop.*, vol. AP-26, no. 4, pp. 442 - 446, July.

Balanis, C. A. 1989, *Advanced Engineering Electromagnetics*, Chapter 11, page 573, Wiley, New York, NY.

Beker, B., K. R. Umashankar, and A. Taflove. 1989. "Numerical Analysis and Validation on the Combined Surface Integral Equations fro Electromagnetic Scattering by Two-Dimensional Anisotropic Objects," *IEEE Trans. Antennas Prop.*, vol. AP-37, no. 12, pp. 1573 - 1581, December.

Beker, B., K. R. Umashankar, and A. Taflove. 1990. "Electromagnetic Scattering by Arbitrarily Shaped Two-Dimensional Perfectly Conducting Objects with Homogeneous Anisotropic Materials," *Electromagnetics*, vol. 10, no. 4, pp. 387-406, December.

Beker, B. 1991. "Scattering and Radiation From Cylindrical Anisotropic Shells," *Proc. Southeast Symposium on System Theory*, pp. 405 - 409, Columbia, SC March.

Beker, B. 1991. "Electromagnetic Field Behavior Near Homogeneous Anisotropic Wedges," *IEEE Trans. Antennas Prop.*, vo. AP-39, no. 8, pp. 1143 - 1151, August.

Graglia, R. D. and P. L. E. Uslenghi. 1987. "Electromagnetic Scattering from Anisotropic Materials, Part II: Computer Code and Numerical Results in Two-Dimesions," *IEEE Trans. Antennas Prop.*, vol. AP-35, no. 2, pp. 225 - 232, February.

Harrington, R. F. 1968. *Field Computation By Moment Mothods*, The Macmillan Company, New York, NY.

Jackson, J. D. 1975. *Classical Electrodynamics*, 2nd ed., Chapter 2, Sec. 2.11, Wiley, New York, NY.

Marx, E. 1990, "Computed Fields Near the Edge of a Dielectric Wedge," *IEEE Trans. Antennas Prop.*, vol. AP-38, no. 9, pp. 1438 - 1442, September.

Monzon, J. C. 1988. "On a Surface Integral Representation for Homogeneous Anisotropic Regions: Two-Dimensional Case," *IEEE Trans. Antennas Prop.*, vol. AP-36, no. 10, pp. 1401 - 1406, October.

Van Bladel, J. 1985. "Field Singularities at Metal-Dielectric Wedges," IEEE Trans. Antennas Prop., vol. AP-33, no. 4, pp. 450 - 455, April.

Umashankar, K. R. and A. Taflove. 1984. "Analytical Models for Electromagnetic Scattering," Final Report to Electromagnetic Science Division., RADC, Hanscom AFB (June), MA.

Appendix

Input/Output File Samples of MOM for Anisotropic Cylindrical Shells

The input section of the SHELL.FOR file:

```
      PROGRAM SHELL

C.....................................................................
C                                                                      .
C   This program computes induced surface currents and radiated        .
C fields of a dielectric and/or permeable cylinder coated with a       .
C single LOSSY layer of anisotropic material. The composite            .
C scatterer is excited by a TM-polarized line source located           .
C inside the bulk region.                                              .
C                                                                      .
C  Note:  The magnitude of line source |Ezi| = 1.0 V/m                 .
C       For TE polarization use duality: Ez -> Hz,                     .
C       [eps] -> [mu], and [mu] -> [eps].                              .
C.....................................................................
C                                                                      .
C Author: Benjamin Beker                                               .
C         Dept. of Electrical & Computer Engineering                   .
C         University of South Carolina                                 .
C         Columbia, SC 29208                                           .
C         (803) 777-3469                                               .
C       E-mail: beker@charlie.ece.scarolina.edu                        .
C.....................................................................

C
C            .... Main Program Input....
C

C
C ........... Relative medium constants .....................
C
C .... Index 1 corresponds to the external medium and index 2
C              to the internal dielectric core....
C

      FREQ   = 4.0E+08
      EPS(1) = 1.0
      MU(1)  = 1.0
      EPS33  = CMPLX( 1.0 , 0.0 )
      MU11   = CMPLX( 5.0 , 0.0 )
      MU22   = CMPLX( 4.5 , - 0.005 )
      MU12   = CMPLX( 0.0 , 0.0 )
      EPS(2) = 1.0
      MU(2)  = 1.0

C.....................................................................
C                                                                      .
C  N(1) -------> # of unknown current pulses on the ext.               .
```

```
C                scatterer for each of the currents          .
C                                                            .
C  N(2) -------> # of unknown current pulses on the int.     .
C                scatterer for each of the currents          .
C                                                            .
C  NOTE:         neither n(1) or n(2) should exceed 150      .
C                unless the matrix arrays are redimensioned  .
C                                                            .
C  NCP(1) -----> # of contour points on the ext. scatterer   .
C                                                            .
C  RA(1) ------> radius of the ext. circle in meters         .
C                                                            .
C  RA(2) ------> radius of the int. circle in meters         .
C                                                            .
C  NL    ------> # of contours (currently NL = 2 which       .
C                corresponds to a shell)                     .
C                                                            .
C............................................................
```

```
      N(1)  = 120
      N(2)  = 120
      RA(1) = 0.1254
      RA(2) = 0.1
      NL    = 2
```

The output file FOR018.DAT:

```
            TE-Scattering Data
        --------------------------------

 Pulse        Real Part      Imag. Part         Magnitude

              ------ Mz (Ext. Contour) -----

    1        -0.0022386       0.0030364       1.4221663
    2        -0.0022378       0.0030355       1.4216969
    3        -0.0022361       0.0030335       1.4207293
    4        -0.0022335       0.0030307       1.4193100
    5        -0.0022302       0.0030270       1.4174374
    6        -0.0022261       0.0030224       1.4151201
    7        -0.0022213       0.0030170       1.4123945
    8        -0.0022157       0.0030108       1.4092689
    9        -0.0022096       0.0030038       1.4057910
   10        -0.0022029       0.0029962       1.4019868

   55        -0.0022261       0.0030224       1.4151261
   56        -0.0022302       0.0030270       1.4174254
   57        -0.0022335       0.0030308       1.4193202
   58        -0.0022361       0.0030335       1.4207281
   59        -0.0022378       0.0030355       1.4216964
   60        -0.0022386       0.0030364       1.4221785
   61        -0.0022386       0.0030364       1.4221652
   62        -0.0022378       0.0030355       1.4217049
   63        -0.0022360       0.0030335       1.4207244
   64        -0.0022336       0.0030308       1.4193224
   65        -0.0022302       0.0030270       1.4174256

  110        -0.0021957       0.0029880       1.3978842
```

111	-0.0022029	0.0029962	1.4019806
112	-0.0022096	0.0030038	1.4057915
113	-0.0022157	0.0030108	1.4092811
114	-0.0022212	0.0030170	1.4123819
115	-0.0022261	0.0030224	1.4151254
116	-0.0022302	0.0030270	1.4174368
117	-0.0022335	0.0030307	1.4193102
118	-0.0022360	0.0030336	1.4207398
119	-0.0022378	0.0030354	1.4216809
120	-0.0022386	0.0030364	1.4221810

------ Js (Ext. Contour) -----

121	1.0492311	-0.6342636	1.2260408
122	1.0490825	-0.6343570	1.2259620
123	1.0486403	-0.6346370	1.2257285
124	1.0479072	-0.6350989	1.2253408
125	1.0468915	-0.6357400	1.2248049
126	1.0456034	-0.6365533	1.2241269
127	1.0440555	-0.6375290	1.2233131
128	1.0422623	-0.6386582	1.2223728
129	1.0402439	-0.6399286	1.2213173
130	1.0380151	-0.6413270	1.2201540
175	1.0440561	-0.6375304	1.2233144
176	1.0456054	-0.6365552	1.2241296
177	1.0468925	-0.6357415	1.2248065
178	1.0479070	-0.6351005	1.2253414
179	1.0486450	-0.6346405	1.2257345
180	1.0490789	-0.6343566	1.2259587
181	1.0492308	-0.6342649	1.2260413
182	1.0490873	-0.6343607	1.2259680
183	1.0486403	-0.6346380	1.2257291
184	1.0479070	-0.6351004	1.2253414
185	1.0468932	-0.6357417	1.2248074
230	1.0330383	-0.6444526	1.2175744
231	1.0356061	-0.6428420	1.2189035
232	1.0380172	-0.6413302	1.2201574
233	1.0402443	-0.6399315	1.2213192
234	1.0422643	-0.6386592	1.2223749
235	1.0440576	-0.6375302	1.2233156
236	1.0456040	-0.6365535	1.2241275
237	1.0468916	-0.6357406	1.2248054
238	1.0479085	-0.6351001	1.2253426
239	1.0486411	-0.6346372	1.2257293
240	1.0490836	-0.6343574	1.2259631

------ Mz (Int. Contour) -----

241	-0.0028280	0.0027539	1.4881147
242	-0.0028276	0.0027535	1.4879004
243	-0.0028268	0.0027526	1.4874673
244	-0.0028257	0.0027514	1.4868546
245	-0.0028243	0.0027498	1.4860368
246	-0.0028225	0.0027478	1.4850240
247	-0.0028204	0.0027454	1.4838473
248	-0.0028181	0.0027428	1.4825174
249	-0.0028154	0.0027399	1.4810292
250	-0.0028126	0.0027366	1.4794073

295	-0.0028225	0.0027478	1.4850277
296	-0.0028243	0.0027498	1.4860350
297	-0.0028258	0.0027514	1.4868593
298	-0.0028268	0.0027526	1.4874625
299	-0.0028276	0.0027535	1.4879123
300	-0.0028280	0.0027539	1.4881091
301	-0.0028280	0.0027539	1.4881020
302	-0.0028276	0.0027535	1.4879084
303	-0.0028269	0.0027526	1.4874744
304	-0.0028258	0.0027514	1.4868551
305	-0.0028243	0.0027498	1.4860313
350	-0.0028096	0.0027331	1.4776763
351	-0.0028126	0.0027366	1.4794093
352	-0.0028155	0.0027398	1.4810289
353	-0.0028181	0.0027429	1.4825237
354	-0.0028204	0.0027455	1.4838436
355	-0.0028225	0.0027478	1.4850290
356	-0.0028243	0.0027498	1.4860337
357	-0.0028257	0.0027514	1.4868461
358	-0.0028269	0.0027526	1.4874763
359	-0.0028276	0.0027535	1.4879031
360	-0.0028280	0.0027539	1.4881083

------ Js (Int. Contour) -----

361	2.1365283	0.2950120	2.1567998
362	2.1365638	0.2950518	2.1568403
363	2.1366673	0.2951703	2.1569591
364	2.1368406	0.2953671	2.1571577
365	2.1370780	0.2956393	2.1574302
366	2.1373813	0.2959845	2.1577780
367	2.1377437	0.2963988	2.1581938
368	2.1381588	0.2968771	2.1586707
369	2.1386247	0.2974153	2.1592062
370	2.1391389	0.2980073	2.1597972
425	2.1370809	0.2956388	2.1574330
426	2.1373799	0.2959833	2.1577764
427	2.1377499	0.2963982	2.1581998
428	2.1381590	0.2968758	2.1586707
429	2.1386256	0.2974134	2.1592069
430	2.1391463	0.2980063	2.1598043
431	2.1396866	0.2986447	2.1604276
432	2.1402729	0.2993254	2.1611023
433	2.1408827	0.3000392	2.1618054
434	2.1415083	0.3007784	2.1625276
435	2.1421559	0.3015370	2.1632745
470	2.1402714	0.2993243	2.1611009
471	2.1396878	0.2986449	2.1604288
472	2.1391366	0.2980057	2.1597946
473	2.1386251	0.2974140	2.1592064
474	2.1381588	0.2968763	2.1586707
475	2.1377399	0.2963975	2.1581898
476	2.1373787	0.2959838	2.1577752
477	2.1370776	0.2956391	2.1574297
478	2.1368382	0.2953668	2.1571553
479	2.1366663	0.2951705	2.1569581
480	2.1365628	0.2950521	2.1568394

Angle	Scatt. Field	RCS	RCS(dB)	Norm. Power
360.00	1.5925131	1.1949408	0.7734638	3.9869463
359.00	1.5825242	1.1949575	0.7735247	3.9870071
358.00	1.5825577	1.1950082	0.7737056	3.9871910
357.00	1.5826125	1.1950909	0.7740095	3.9874921
356.00	1.5826898	1.1952076	0.7744335	3.9879155
355.00	1.5827891	1.1953576	0.7749784	3.9884610
175.00	1.5827912	1.1953608	0.7749902	3.9884725
174.00	1.5829117	1.1955429	0.7756516	3.9891341
173.00	1.5830539	1.1957577	0.7764319	3.9899142
172.00	1.5832180	1.1960056	0.7773319	3.9908144
171.00	1.5834035	1.1962858	0.7783495	3.9918318
170.00	1.5836093	1.1965969	0.7794787	3.9929612
169.00	1.5838367	1.1969404	0.7807255	3.9942081
168.00	1.5840840	1.1973144	0.7820820	3.9955645
167.00	1.5843515	1.1977187	0.7835486	3.9970310
166.00	1.5846393	1.1981540	0.7851261	3.9986088
165.00	1.5849469	1.1986190	0.7868118	4.0002942
5.00	1.5827889	1.1953574	0.7749777	3.9884601
4.00	1.5826900	1.1952080	0.7744348	3.9879172
3.00	1.5826129	1.1950915	0.7740115	3.9874940
2.00	1.5825579	1.1950085	0.7737099	3.9871922
1.00	1.5825242	1.1949575	0.7735247	3.9870071
0.00	1.5825129	1.1949404	0.7734625	3.9869452

REPORT DOCUMENTATION PAGE

Form Approved
OMB No. 0704-0188

1. AGENCY USE ONLY (Leave blank)	2. REPORT DATE	3. REPORT TYPE AND DATES COVERED
	March 1993	Final: Summer 1992

4. TITLE AND SUBTITLE

APPLICATION OF INTEGRAL AND DIFFERENTIAL EQUATION METHODS FOR VARIOUS EM INTERACTION PROBLEMS

5. FUNDING NUMBERS

PE: 0602121N
TA: RH21C13

6. AUTHOR(S)

7. PERFORMING ORGANIZATION NAME(S) AND ADDRESS(ES)

University of South Carolina
Columbia, SC 29208

8. PERFORMING ORGANIZATION REPORT NUMBER

9. SPONSORING/MONITORING AGENCY NAME(S) AND ADDRESS(ES)

Office of Naval Technology
ONT-211
Arlington, VA 22217-5000

Naval Command, Control and Ocean Surveillance Center (NCCOSC)
RDT&E Division
San Diego, CA 92152-5001

10. SPONSORING/MONITORING AGENCY REPORT NUMBER

TD 2453

11. SUPPLEMENTARY NOTES

12a. DISTRIBUTION/AVAILABILITY STATEMENT

Approved for public release; distribution is unlimited.

12b. DISTRIBUTION CODE

13. ABSTRACT *(Maximum 200 words)*

This document reviews the application of integral equation methods that are commonly used to study the interaction of EM fields with two-dimensional lossy anisotropic objects. The study focuses on plane wave scattering done by arbitrarily shaped cylindrical geometries that have circular and rectangular cross sections. In addition to discussing solid material objects, the document investigates the bistatic radar cross section of several metallic circular cylinders that are coated with a single layer of anisotropic material. The document concludes by investigating the radiation effects from a uniform line source that runs through a lossy anisotropic shell of finite thickness.

The document discusses combined-field surface integral equations (CFSIEs). It presents highlights of the method of moments (MOM) numerical solution to CFSIEs and gives numerical results for solid, hollow, and coated cylindrical scatterers. The effects of material anisotrophy in the EM response of the scatterer are emphasized.

14. SUBJECT TERMS

integral equations
anisotrophy
method of moments (MOM)
plane wave scattering
radiation
combined-field surface integral equations (CFSIEs)

15. NUMBER OF PAGES

44

16. PRICE CODE

17. SECURITY CLASSIFICATION OF REPORT	18. SECURITY CLASSIFICATION OF THIS PAGE	19. SECURITY CLASSIFICATION OF ABSTRACT	20. LIMITATION OF ABSTRACT
UNCLASSIFIED	UNCLASSIFIED	UNCLASSIFIED	SAME AS REPORT

21a. NAME OF RESPONSIBLE INDIVIDUAL	21b. TELEPHONE *(Include Area Code)*	21c. OFFICE SYMBOL
S. T. Li, COTR	(619) 553-5089	Code 824

INITIAL DISTRIBUTION

Code 0012	Patent Counsel	(1)
Code 0141	A. Gordon	(1)
Code 0244	V. Ware	(1)
Code 80	K. D. Regan	(1)
Code 805	J. W. Rockway	(1)
Code 82	R. J. Kochanski	(1)
Code 824	J. B. Rhode	(1)
Code 824	C. A. Deneris	(1)
Code 824	J. Ho	(1)
Code 824	L. B. Koyama	(1)
Code 824	S. T. Li	(1)
Code 824	J. C. Logan	(10)
Code 824	A. Page	(1)
Code 824	J. H. Schukantz	(1)
Code 824	D. W. Tam	(1)
Code 961	Archive/Stock	(6)
Code 964B	Library	(2)

Defense Technical Information Center
Alexandria, VA 22304-6145 (4)

Center for Naval Analyses
Alexandria, VA 22302-0268

GIDEP Operations Center
Corona, CA 91718-8000

Office of the Chief of Naval Research
Arlington, VA 22217-5000

Naval Sea Systems Command
Washington, DC 20362-5101 (2)

U. S. Army Information Systems
Engineering & Integration Center
Fort Huachuacha, AZ 85613-7300

University of South Carolina
Columbia, SC 29208 (10)

NCCOSC Washington Liaison Office
Washington, DC 20363-5100

Navy Acquisition, Research &
Development Information
Center (NARDIC)
Washington, DC 20360-5000

NCCOSC Division Detachment
Warminster, PA 18974-5000

Space and Naval Warfare
Systems Command
Washington, DC 20363-5100 (4)

Naval Surface Warfare Center
Carderock Division
Bethesda, MD 20084-5000

Naval Postgraduate School
Monterey, CA 93940-5000